SPATIOTEMPORAL TESTING AND MODELING OF CATFISH RETINAL NEURONS

HOWARD I. KRAUSZ AND KEN-ICHI NAKA, *Department of Physiology and Biophysics, University of Texas Medical Branch, Galveston, Texas 77550 U.S.A.*

ABSTRACT The responses of retinal neurons depend on the interaction of both temporal and spatial aspects of a light stimulus. We developed a linear spatiotemporal model of receptor and horizontal cell layers in the catfish retina based on reciprocal interactions between both layers and coupling within each. Horizontal cell transfer properties were measured experimentally using white-noise intensity modulated light spots of different diameters and were compared with analytical predictions based on the model. Good agreement was obtained with a reasonable choice of model space-constants and feedback parameters. Furthermore, the same set of parameter values determined from spot experiments enabled accurate prediction of experimental horizontal cell responses to traveling gratings. The proposed feedback connections from horizontal cells to receptors quicken the time-course of responses in both layers and sharpen receptive fields.

INTRODUCTION

In the first stages of visual perception, the changing pattern of light intensity focused on the retina is transformed into receptor and horizontal cell potential. This manuscript is intended as a step toward the development of a functionally accurate description of these transformations.

Both spatial and temporal aspects of retinal organization must be considered simultaneously since the spatial extent of a light stimulus will generally affect the time-course of responses to changes in its intensity. For example, receptor (Baylor et al., 1971) and horizontal cell (Marmarelis and Naka, 1973*a,b*) responses to small circular spots become faster in waveform as spot area is increased.

Various authors have suggested that horizontal cell feedback to receptors accounts for these observations, but the nature of the interaction between feedback and direct signals remains to be clarified. Fukurotani and Hara (1975) used an iterative computer simulation to demonstrate that subtraction of horizontal cell potential from receptor potential can mimic the effects of spot area on horizontal cell response waveform. We decided to test this subtractive feedback hypothesis under more general experimental stimulus conditions by first incorporating feedback into an overall spatiotemporal model.

The theoretical section of this paper begins with existing models of the steady-state spatial distribution of horizontal cell potential and then includes the temporal dynamics of phototransduction and of forward and proposed feedback connections between receptors and

---

Dr. Krausz's present address is Ph.D. to M.D. Program, University of Miami School of Medicine, Miami, Fla. 33152. Dr. Naka's present address is National Institute of Basic Biology, Okazaki, Japan 444.

horizontal cells. Analytic solutions are found for predicted spatiotemporal transfer functions relating electrical potential output from each cell population to light input.

The results of various experimental tests of the spatiotemporal properties of horizontal cell potential are in good agreement with the predictions of the subtractive feedback model, yet some problems remain. These are discussed, and an alternative feedback model is proposed.

THEORETICAL ANALYSIS

Existing models of external horizontal cells in various retinas (Naka and Rushton, 1967; Marmarelis and Naka, 1972; Lamb, 1976; Nelson, 1977) treat the entire cell layer as a flat electrically coupled "S-space" in which potentials diffuse laterally and sum linearly. Since the thickness, d, of the lamina is small (<0.05 mm), the variation of S-potential with depth is negligible (Marmarelis and Naka, 1972). For a radially symmetric stimulus, horizontal cell potential V, expressed in polar coordinates, will depend only on position, r, and time, t, according to Bessel's equation (Jack et al., 1975; Kreider et al., 1966):

$$\nabla^2 V(r, t) = \frac{1}{r} \frac{\partial}{\partial r}\left(r \frac{\partial V(r, t)}{\partial r}\right) = \frac{\rho_i}{d} J(r, t), \tag{1}$$

where $J(r, t)$ is the total transmembrane current density and ρ_i is the internal resistivity of the S-space.

The transmembrane current density may be broken into three components:

$$J(r, t) = \frac{2V(r, t)}{\rho_m} + 2c_m \frac{\partial V(r, t)}{\partial t} - j(r, t), \tag{2}$$

where the first two terms in Eq. 2 denote the current density that flows passively through the resistance and capacitance, respectively, of both bounding membranes and $j(r, t)$ represents the change in transmembrane current density induced by changes in receptor potential. For inward current, $j(r, t)$ is considered to be positive and $V(r, t)$ decreases or hyperpolarizes.

Horizontal cells in catfish retina respond nearly linearly to small fluctuations in light intensity about a fixed mean level (Marmarelis and Naka, 1973*a*,*b*). Since the assumption of linearity greatly simplifies the modeling task, we restrict the range of applicability of the model to linear responses and assume that fluctuations in horizontal and receptor potentials about their respective means are linear functions of the light input modulation.

In the frequency domain the linear relation between receptor potential fluctuations and horizontal cell input may be expressed as

$$\frac{1}{2} \rho_m \hat{j}(r, f) = \hat{A}(f) \hat{U}(r, t), \tag{3}$$

where $\hat{U}(r, f)$ is the Fourier transform of receptor potential at location r and $\hat{A}(f)$ is the transfer function between receptors and horizontal cells.

When Eqs. 1 and 2 are transformed into the frequency domain and combined with Eq. 3, the result is

$$\alpha^2 \nabla^2 \hat{V}(r, f) - (1 + i2\pi\rho_m c_m f) \hat{V}(r, f) = -\hat{A}(f) \hat{U}(r, f), \tag{4}$$

where $\alpha^2 = \rho_m d / 2\rho_i$.

Now that horizontal cell potential fluctuations have been related to receptor potential through Eq. 4, we proceed to model the effect of a light stimulus on receptor potential. When a fixed, radially symmetric stimulus pattern is modulated in intensity about some mean, $\bar{I}$, the incident light intensity at position r is modulated by:

$$I(r, t) = \bar{I}i(t)\, p(r), \tag{5}$$

where $i(t)$ is the temporal modulation depth and $p(r)$ is zero for areas of steady illumination (or no illumination) and unity for areas receiving the maximum modulation.

A stimulus modulation defined by Eq. 5 will give rise to a receptor potential fluctuation that satisfies:

$$\hat{U}(r,f) = m(\bar{I})\hat{g}(f)I(r, t) = m(\bar{I})\bar{I}\hat{g}(f)\hat{i}(f)\, p(r), \tag{6}$$

where $\hat{g}(f)$ is the transfer function of the linear stages of phototransduction and $m(\bar{I})$ is the slope of the nonlinear Michaelis relation believed to follow the linear receptor processes (Baylor et al., 1974). In general, $m(\bar{I})$ will vary with position r, but by allowing a suitable redefinition of $p(r)$ when necessary, $m(\bar{I})$ can be kept constant.

Any feedback effects due to horizontal cell activity will combine with the direct effects of light on receptor potential. If the horizontal cell signal at each location r is filtered with transfer function $\hat{k}(f)$ and fed back negatively to the nearest receptor, then Eq. 6 changes to:

$$\hat{U}(r,f) = m(\bar{I})\bar{I}p(r)\hat{g}(f)\hat{i}(f) - \hat{k}(f)\hat{V}(r,f), \tag{7}$$

The two Eqs. 4 and 7, describing horizontal and receptor potentials, take a simpler form when new variables are defined for each cell layer. For receptors, let

$$\Phi(r,f) = \frac{\hat{U}(r,f)}{m(\bar{I})\bar{I}\hat{g}(f)\hat{i}(t)} \tag{8}$$

and let

$$\Psi(r,f) = \frac{\hat{V}(r,f)}{m(\bar{I})\bar{I}\hat{i}(f)\hat{g}(f)\hat{A}(f)} \tag{9}$$

be the corresponding horizontal cell variable.

In terms of these new transfer functions, Eqs. 7 and 4 become:

$$\Phi(r,f) = p(r) - \hat{k}(f)\hat{A}(f)\Psi(r,f) \tag{10}$$

$$\alpha^2\nabla^2\Psi(r,f) - (1 + i2\pi\rho_m c_m f)\Psi(r,f) = -\Phi(r,f). \tag{11}$$

Finally substitution of Eq. 10 into Eq. 11 gives a single Bessel equation:

$$\nabla^2\Psi - \frac{1}{\lambda^2(f)} = -\frac{p(r)}{\alpha^2}, \tag{12}$$

where the "space-constant" $\lambda(f)$ is:

$$\lambda^2(f) = \frac{\alpha^2}{1 + i2\pi\rho_m c_m f + \hat{A}(f)\hat{k}(f)}. \tag{13}$$

The basic assumptions and variable defintions leading to Eqs. 12 and 13 are diagrammed in Fig. 1. Receptors transduce light independently in blocks labeled tentatively as "outer segments." In the region labeled "inner segments," outer-segment signals combine with feedback signals from horizontal cells. The result is the measured receptor signal $U(r, t)$, which provides the input to the S-space. In our basic model, no coupling of receptor signals is assumed, but receptor coupling is included in the more complete theory of Appendix A.

Green's Function Solution

A common method for solving an inhomogenous linear differential equation such as Eq. 12 is to construct a Green's function or impulse response function $G(r, s)$. With the aid of Dettman (1969) and Kreider et al. (1966), we derived the solution:

$$G(r, s) = \begin{cases} I_0(r/\lambda)K_0(s/\lambda) & r < s \\ K_0(r/\lambda)I_0(s/\lambda) & r > s, \end{cases} \tag{14}$$

where I_0 and K_0 are modified Bessel functions of order zero. Given the Green's function, the solution to Eq. 15 is given by the convolution integral:

$$\Psi(r, f) = \frac{1}{\alpha^2} \int_0^\infty p(s)G(r, s)s\,ds. \tag{15}$$

As a specific example of immediate relevance, consider a uniformly illuminated circular spot stimulus of radius R on a dark background. Then,

$$p(s) = \begin{cases} 1, & s < R \\ 0, & s > R. \end{cases} \tag{16}$$

By consulting a table of Bessel function identities (as in Carslaw and Jaeger, 1959, or Abramowitz and Stegun, 1965) the resulting convolution integral (Eq. 15) may be evaluated,

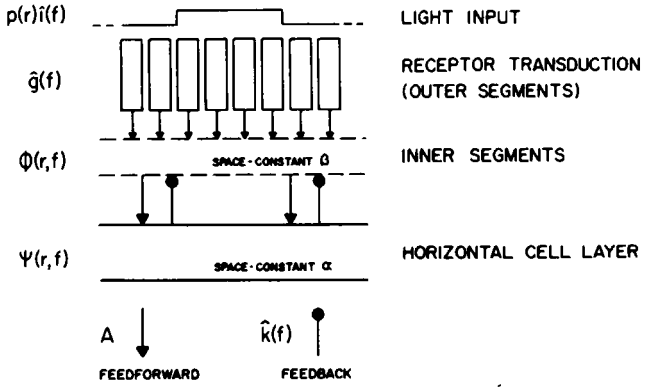

FIGURE 1 Diagram of model circuitry. Receptors transduce light input linearly and independently, with transfer function $\hat{g}(f)$. Receptor inner segments and horizontal cells interact by feedforward connections (gain A, no filtering) and feedback connections (transfer function $\hat{k}(f)$). In the basic model, only horizontal cells are assumed to be coupled, while receptor coupling after transduction is incorporated in the more general formulation.

yielding the result:

$$\Psi(r,f) = \frac{1}{\alpha^2} F(r, R, \lambda),$$

where

$$F(r, R, \lambda) = \begin{cases} \lambda^2[1 - (R/\lambda)I_0(r/\lambda)K_1(R/\lambda)] & r < R \\ \lambda R I_1(R/\lambda)K_0(r/\lambda) & r > R. \end{cases} \quad (17)$$

Knowing $\Psi(r,f)$ the receptor transfer function $\Phi(r,f)$ follows from Eq. 10.

In Appendix A the model solution (Eq. 17) is extended to cases where fixed parameters may assume different values inside or outside of a modulated light spot. Receptor coupling is also treated. Appendix B relaxes the requirement that the stimulus be radially symmetric and derives a formula analogous to Eq. 17, but for one-dimensional moving grating stimuli.

Properties of the Solution

The formula in Eq. 17 describes the predicted dependence of horizontal cell potential changes on position r and spot radius R. Outside of a modulated spot stimulus ($r > R$), Eq. 17 predicts that the amplitude of horizontal cell response modulations will decay with distance according to $K_0(r/\lambda)$. Clearly, λ is the effective space-constant in this situation.

This result is completely analogous to the decay of steady-state horizontal cell potential analyzed by Naka and Rushton (1965) and others, with one significant exception. In the case of intensity-modulated stimuli, the space-constant λ is not a single constant, but rather a varying parameter whose values depend on the temporal frequency of light input modulation according to Eq. 13.

Thus Eq. 17 is a spatiotemporal model where the spatial distribution of horizontal cell potential depends on the time-course of the light stimulus. Likewise, the time-course of horizontal cell response depends on the spatial extent of a stimulus and on its retinal position with respect to the recording electrode. Space and time cannot be considered separately in the model.

Comparison of Model to Experiment

The model solution (Eq. 17) predicts the transfer function $\Psi(r,f)$ for the case of a circular spot stimulus. From its definition (Eq. 9), an experimental determination of $\Psi(r,f)$ requires measurement of the light-to-horizontal cell transfer function $\hat{V}(r,f)/\hat{\imath}(f)$ and of the product of $\hat{g}(f)$ and $\hat{A}(f)$. Neither the phototransduction transfer function, $\hat{g}(f)$, nor the receptor-to-horizontal cell transfer function, $\hat{A}(f)$, is readily accessible to measurement. Their product is the light-to-horizontal cell transfer function in the absence of feedback, but feedback is difficult to eliminate reliably.

So in view of these considerations, the best approach is not to measure $\Psi(r,f)$, but rather to compare ratios of transfer functions for two different spot radii instead. From Eqs. 9 and 17:

$$\frac{\Psi(r,f)|_{R=R_1}}{\Psi(r,f)|_{R=R_2}} = \frac{[\hat{V}(r,f)/\hat{\imath}(f)]_{R=R_1}}{[\hat{V}(r,f)/\hat{\imath}(f)]_{R=R_2}} = \frac{F(r, R_1, \lambda)}{F(r, R_2, \lambda)} \quad (18)$$

When a spot of radius R is compared with a full field stimulus ($R_2 = \infty$), it may be shown that

$$\frac{\Psi(r,f)_{\text{spot}}}{\Psi(r,f)_{\text{field}}} = \frac{1}{\lambda^2} F(r, R, \lambda). \tag{19}$$

The left side of Eq. 19 may be estimated experimentally by dividing spot and field horizontal cell transfer functions, as indicated by Eq. 18. This ratio of the two transfer functions equals $\hat{V}(r,f)_{\text{spot}}/\hat{V}(r,f)_{\text{field}}$, which is the transfer function of a hypothetical linear filter that converts horizontal cell field responses into spot responses. The right side of Eq. 19 is a mathematical expression based on the model and depends on only one unspecified parameter $\lambda(f)$, which itself is a function of frequency.

Given fixed values of r and R, the model can be made to fit the experimental ratio by a proper choice of $\lambda(f)$ in Eq. 19, thereby providing experimental estimates of the model quantities $\Psi(r,f)$ and $\lambda(f)$. When the basic model is generalized to include receptor coupling or different parameter values inside and outside the stimulating spot, the field-to-spot transfer function in Eq. 19 is equal to a corresponding expression derived from Appendix A.

METHODS

Experimental Animals

Eyes from Texas channel catfish (*Ictalurus punctatus*) were removed and hemisected. The posterior "eye-cup" half was placed in a small chamber supplied with moist oxygen gas and mounted on a firm support.

Recording

Intracellular recordings from external horizontal cells were made according to procedures previously described by Naka and Nye (1970). Horizontal cell responses were identified by their characteristic response to square pulse light stimulation.

Stimulation

In one set of experiments the light stimulus pattern was either a circular spot 200 μm diam or a large, uniformly illuminated field (3 mm diam). The stimulating spot was centered over the electrode by adjusting its position until the step response was maximal. Spot and field stimulus patterns were then modulated in intensity in Gaussian white-noise fashion about a fixed mean level.

The modulating signal typically lasted ~1 min and had a flat power spectrum from near DC up to ~50 Hz. The depth of modulation, defined as the standard deviation divided by the mean intensity was kept to ~25%. This stimulus enabled us to test the system rapidly over a range of nearly linear responses. Furthermore, Gaussian white-noise inputs have the additional advantage (discussed later) that memoryless nonlinearities do not affect the waveform of input-output crosscorrelation (Korenberg, 1973; Marmarelis and Marmarelis, 1978).

A second set of experiments was performed with a moving one dimensional, white-noise grating stimulus according to the method of Yasui et al. (1979). The mean intensities in those experiments corresponded approximately to the intensities of spot or field illumination.

The retinas were adapted to ordinary room light but experiments were performed in the absence of any background illumination.

Data Analysis

First and occasionally second kernels were computed from the crosscorrelation formulas (Lee and Schetzen, 1965):

$$h_1(\tau) = \frac{1}{P} E\{y(t)x(t-\tau)\}$$

$$h_2(\tau_1, \tau_2) = \frac{1}{2P^2} E\{y(t)x(t-\tau_1)x(t-\tau_2)\} \quad \tau_1 \neq \tau_2, \tag{20}$$

where $x(t)$ is the white-noise input, $y(t)$ is the response, P is the power density of the noise and $E\{\ \}$ denotes time average or expected value. The GAS system of programs by Dale Knutsen (California Institute of Technology, Pasadena, Calif.) was used for kernel computation.

In the case of the moving grating stimulus, $x(t)$ was taken as the intensity modulation signal in time measured at a fixed point on the retina. The deviation between this fixed point and the electrode location merely introduced an arbitrary time shift in the measured kernels. Moving grating kernels were Fourier transformed and divided by the autospectrum of the input signal to correct for slight deviations in the autospectrum from true flatness.

To compare spot and field kernels with model predictions, kernels were Fourier transformed and the resulting spot transfer function was divided by the field kernel transform, yielding a field-to-spot transfer function.

Generation of Model Responses and Fitting of Model to Data

The predictions of all of the various model equations were simulated by computer. The various parameters associated with each equation could be assigned fixed values or given initial values that were varied automatically. A modified Levenberg-Marquardt nonlinear least-squares fitting algorithm (Brown and Dennis, 1972) was used to adjust the variable parameters of a given model until the difference between experimental results and model predictions was minimized.

RESULTS

Fig. 2 compares six horizontal cell kernels measured from three different cells using a 200-μm-diam spot stimulus (Fig. 2 *A*), or full field illumination (Fig. 2 *B*), all normalized to the same amplitude. The field kernels always peak sooner, repolarize faster and are less damped (more oscillatory), than spot kernels.

Spot and field kernels from one of the cells shown in Fig. 2 are both replotted on the same scale in Fig. 3 *A*, where the field kernel is now seen to be much larger in amplitude than the spot kernel due to the summating effects of horizontal cell coupling. The slower time-course of spot kernels compared with field kernels is also evident from a plot of the magnitudes of Fourier transformed kernels, since the spot transfer function (Fig. 3 *B*) falls off at a lower cutoff frequency than does the field transfer function. The kernel transforms show slight resonant peaks, indicative of underdamping, as has also been observed in carp (Toyoda, 1974; Fukurotani and Hara, 1975).

The spot and field horizontal cell first kernels (Fig. 3 *A*) served to predict the corresponding horizontal cell output with reasonable accuracy, so we concluded that horizontal cell responses are nearly linear under these circumstances, as found earlier by Marmarelis and Naka (1973*b*). Nonlinear distortions appeared to be of the memoryless type.

To compare the experimental first kernels in Fig. 3 with model predictions, spot and field

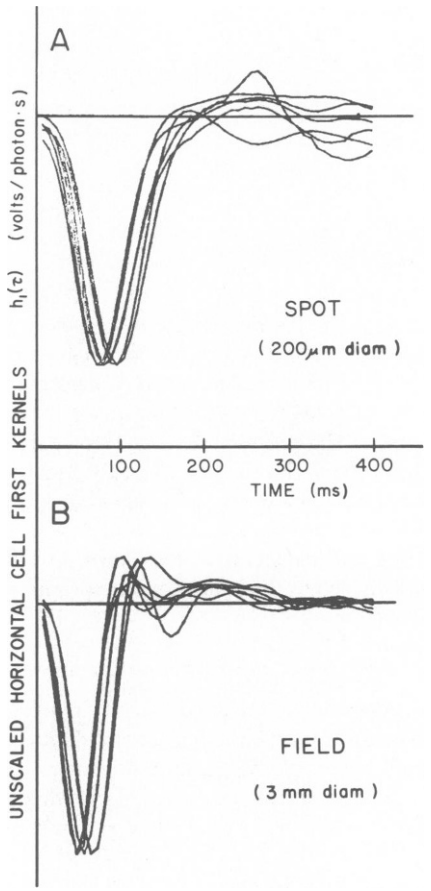

FIGURE 2 Spot and field kernels. All kernels are normalized to the same amplitude and depolarizaton is plotted upwards. (A) Horizontal cell kernels for fixed centered spot stimuli white-noise modulated in intensity. Kernels from three different cells are shown with two repetitions for each cell. Spot diameter was 200 μm. (B) Kernels for the same three cells as in A but with spot diameter enlarged to 2 mm (full field illumination.

kernel transforms must first be divided as explained on page 17. The resulting field-to-spot transfer function appears as a Bode plot in Fig. 4 where the wavy lines indicate gain and phase as a function of frequency. The initial low-pass nature of the Bode magnitude plot (Fig. 4 *A*) is a consequence of the fact that spot kernels are slower in time-course than field kernels. However, at high frequencies the gain of this transfer function increases due to the fact that the field kernel gain (Fig. 3) falls more rapidly than spot gain. The actual values of the field-to-spot transfer function at frequencies above ~12 Hz must be regarded as uncertain since the field gain, which appears in the denominator of the ratio, is so greatly attenuated. In spite of minor quantitative differences, the overall features of Fig. 4 are quite repeatable between experiments.

In the basic model with no receptor coupling, the model predicted field-to-spot transfer function is given by Eq. 19, whereas Eqs. A16 and 18 apply in the most general case. Regardless of which formulas apply, the prediction will depend on feedback only through the

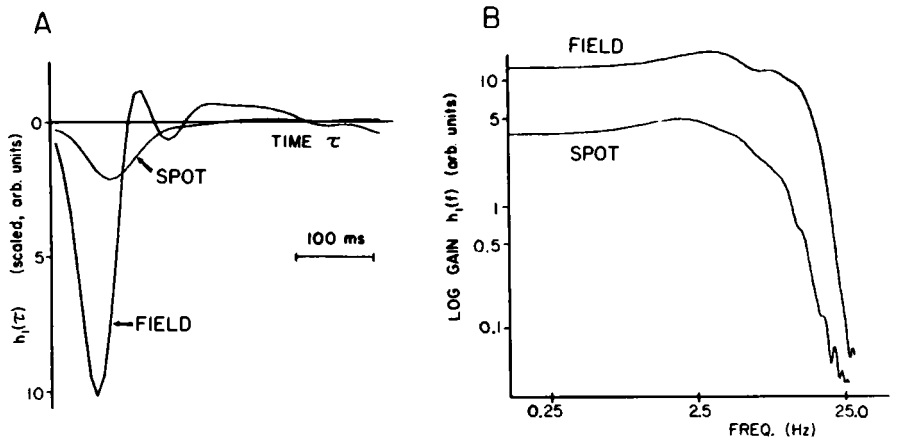

FIGURE 3 Scaled kernels and their gains. (A) Spot and field horizontal cell kernels for one of the cells in Fig. 2, both plotted on the same vertical scale. (B) Gains of spot and field kernels, equal to the magnitudes of the Fourier transforms of kernels in A. Both are drawn to scale. (arb, arbitrary)

product, $\hat{A}(f)\hat{k}(f)$, of feedforward and feedback transfer functions, as is apparent from Eqs. 13, A9, and A10. So from the horizontal cell responses alone, there is no way to distinguish $\hat{A}(f)$ from $\hat{k}(f)$. Therefore, we may make the arbitrary assumption that $\hat{k}(f)$ has unity gain and contains all of the frequency dependence of $\hat{A}(f)\hat{k}(f)$. Then $\hat{A}(f)$ is simply a constant gain A, and model horizontal cell and receptor responses have the same waveform. Preliminary recordings by Eric Lasater[1] indicate that receptor kernels in catfish strongly resemble horizontal cell kernels in waveform and do become faster with larger light spots.

In their simulation of horizontal cell spot kernels, Fukurotani and Hara (1975) assumed a delayed exponential waveform for the feedback impulse response. Similarly, we made the initial estimate that $k(t)$ rises along an S-shaped curve and then decays exponentially. One expression for this standard physiological waveform is (Baylor and Hodgkin, 1974):

$$k(t) = \frac{n+1}{\tau} e^{-(t-t_0)/\tau}[1 - e^{-(t-t_0)/\tau}]^n, \tag{21}$$

where t_0 is the feedback delay, and τ is the feedback time-constant. The corresponding frequency response function is (see Lamb and Simon, 1977):

$$\hat{k}(f) = e^{-i2\pi t_0 f} \prod_{j=1}^{n} (1 + i2\pi fc/j)^{-1} \tag{22}$$

Using the basic model solution (Eq. 17), model parameters were adjusted automatically until the best possible fit to Fig. 4 data was obtained over the range of frequencies from 0 to 12.5 Hz. Two different sets of parameter values, each giving an equally accurate overall fit are listed in columns 1 and 2 of Table I. Model-predicted, field-to-spot transfer functions based on each parameter set appear as smooth lines in Fig. 4. The agreement between experiment and model is satisfactory in both cases.

[1]Lasater, E. Personal communication.

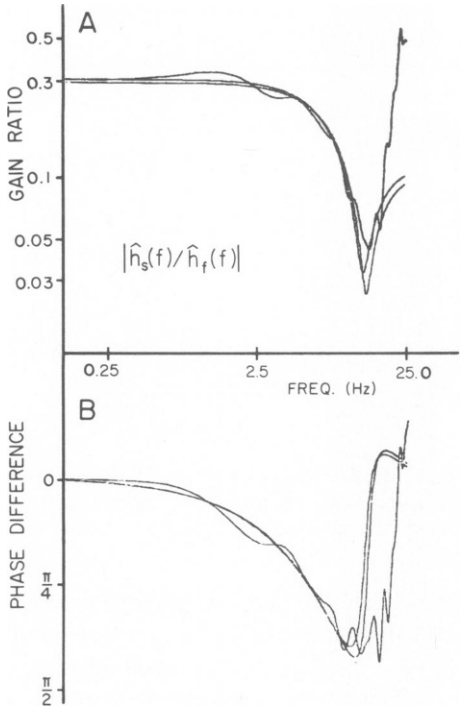

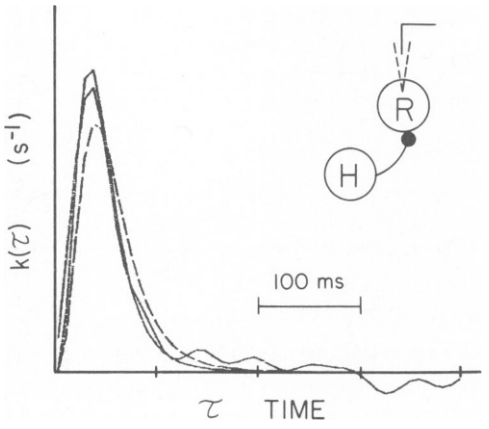

FIGURE 4

FIGURE 5

FIGURE 4 Field-to-spot transfer function shown as a Bode plot. (A) Gain ratio of spot and field kernel transforms. (B) Phase difference between spot and field kernels transforms. Wavy traces are experimental gain and phase found from the ratio of transforms of kernels in Fig. 3. Smooth traces are field-to-spot transfer functions predicted by the basic model using parameters in columns 1 and 2 of Table I.

FIGURE 5 Feedback kernels. The smooth solid trace is the feedback kernel generated by Eq. 18 using the model parameters in Table I, column 4. The smooth dashed trace resulted when feedback gain was assumed to be uniform in space (Table I, column 3 parameters). The wavy trace is the feedback kernel calculated from column 4 parameters by fitting the field-to-spot transfer function (Fig. 4) at each frequency point separately. See text for further explanation.

A comparison of both parameter sets (Table I, columns 1 and 2) should give an idea of the specificity of model parameters. There seems to be a restricted locus of parameter values for which the error of prediction remains minimal. Near this minimum, the model is more sensitive to changes in some parameters than in others, and these sensitivities vary with frequency. The optimal parameter set is unique in the sense that no radically different set of parameter values comes close to fitting the data.

It is also possible to fit the experimental field-to-spot transfer function using the more general solution (Eq. A23), which includes receptor coupling and allows for different parameter values in light and dark regions. An excellent fit was obtained using the parameters in column 3 of Table I with the receptor space-constant β fixed rather arbitrarily to 50 μm. For values of β less than ~50 μm, the effect of increased receptor coupling on model parameters was to decrease the receptor to horizontal cell gain A. This is expected since receptor coupling acts to increase the gain of each receptor by adding the responses of its

TABLE I
MODEL PARAMETER VALUES

		1	2	3	4
α	Horizontal Cell Space-constant, mm	0.267	0.281	0.234	0.257
β	Receptor Space-constant, mm	—	—	0.05	0.05
A_1	Feedback gain in light	3.77	3.99	4.32	2.77
A_2	Feedback gain in dark	3.77	3.99	4.32	0
τ	Feedback time-constant, (ms)	24.8	23.8	48.8	20.0
t_0	Feedback delay, ms	0.022	0.102	0.022	0.354
$\rho_m c_m$	Membrane RC, ms	0	0	0	0
	Relative error	0.21	0.21	0.24	0.16

Values in columns 1 and 2 were found by fitting predictions of the basic model without receptor coupling to the experimental field-to-spot transfer function in Fig. 4. In columns 3 and 4, receptors were assumed to have a coupling constant of 50 μm, and in column 4 feedback gain was set to zero in the dark annular region outside of the stimulating spot.

neighbors to its own. If β is set to values larger than 50 μm, it becomes increasingly difficult to fit the experimental field-to-spot transfer function.

In the parameter set in column 4 of Table I, the feedback gain was set to zero in the dark region outside the modulated light spot. This was done to mimick the finding of Burkhardt (1977) that feedback effects on perch cones in the center of a flashed annulus of light were only observable in the presence of central illumination. In column 3, feedback gain was kept the same in light or darkness.

The feedback time-course corresponding to the parameters in Table I, column 4 appears as a smooth solid line in Fig. 5. The dotted trace in Fig. 5 is the estimated feedback kernel based on the parameters in column 3 of Table I. Since the fitting operations are performed in the frequency domain, these feedback kernels were found by taking the inverse transform of $\hat{k}(f)$ given by Eq. 22.

The membrane resistance capacitance (RC) parameter always has the value of 0 in Table I because large initial estimates of membrane RC were invariably adjusted to very low values by the automatic fitting routines, suggesting that capacitive effects are negligible at frequencies <10 Hz. Capacitive effects increase with frequency in Eq. 13, thereby opposing the action of low-pass feedback pathways.

The agreement between experimental and model curves in Fig. 4 was predicated on the assumption that the feedback kernel is given by Eq. 21. Instead of guessing the shape of $k(t)$, we attempted to compute a time-course for the feedback by fitting the experimental field-to-spot transfer function point by point. Using the parameters in column 4 of Table I, the gain and phase of $\hat{k}(f)$ were adjusted at each value of frequency from $f = 0$ to $f = 18.75$ Hz until model gain and phase computed from Eq. 19 matched experimental gain and phase to within 0.1%.

The inverse Fourier transform of the resulting set of $\hat{k}(f)$ values is shown in Fig. 5 as a solid, wavy line. The small oscillations in $k(t)$ reflect the fact that the $\hat{k}(f)$ values could not be calculated beyond $f = 18.75$ Hz due to the low gain and poor signal:noise ratio of kernel transforms at higher frequencies. This rectangular cutoff in the frequency domain convolves the time domain feedback kernel with the sin x/x function, thereby inducing oscillations with period 1 s/18.75 = 53 ms.

Response to Moving Gratings

All the experimental and model results presented thus far apply only to centered radially symmetric stimulus patterns. Since the theoretical solutions for horizontal and receptor transfer functions also include the dependence of potential on distance, r, between the electrode and the center of the patterns, the theory makes testable predictions about responses to decentered stimuli.

There are a number of experimental difficulties associated with displaced spot experiments. Small modulations of the intensity of a small light spot produce small responses at the center of the spot and even smaller responses in horizontal cells some distance away. Brighter stimulating lights improve the signal:noise ratio but introduce contaminating light scatter and response nonlinearities.

For these experimental reasons, it is more accurate to measure the decay of horizontal cell potentials with distance using bars of light rather than circular spots. One could position a bar at various distances from the recording electrode and measure a kernel using white-noise modulation of the bar's intensity. However, a similar but much simpler experimental approach is to use a moving white-noise grating stimulus developed by Yasui et al. (1979). When this spatial white-noise pattern travels at constant velocity across the retina, the intensity along any line oriented perpendicular to the direction of motion will undergo a white-noise modulation in time. The kernel computed between input light intensity at a fixed location and output horizontal cell response gives the linear approximation of the response to a moving impulse (bar).

The wavy trace labeled "*a*" in Fig. 6 is a horizontal cell kernel measured with a moving

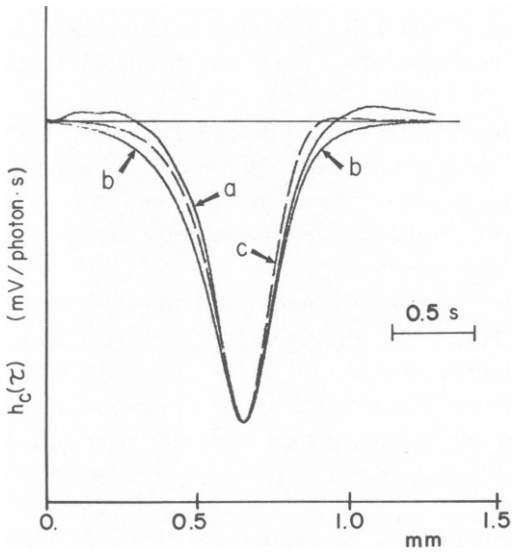

FIGURE 6 Horizontal cell moving grating kernels. (*a*) Measured kernel for a white-noise grating stimulus traveling at a constant velocity of 0.57 mm/s. (*b*) Moving grating kernel predicted from the model based on parameters in Table I, column 4 and on the measured velocity of the grating. (*c*) Kernel predicted from Table I, column 3 parameters.

grating stimulus traveling at a constant velocity measured as 0.57 mm/s. The kernel has been corrected for the deviation between the stimulus autocorrelation and a true impulse, as explained in Methods. Since the kernel represents the response to a moving impulse, one may think of the kernel as a traveling wave of potential that sweeps across the retina following a moving bar. The abscissa in Fig. 6 has units of both time and distance, because the kernel describes both the time-course of potential changes at a fixed retinal location and the spatial extent of the traveling wave.

When the grating is moved at a relatively slow speed, as it was in this experiment, the kernel waveform is determined predominantly by the steady-state, spatial receptive field properties of the horizontal cell. At higher grating velocities, temporal response properties have a greater effect on the kernel waveform. The significant and reproductible features of horizontal cell moving grating kernels are the shapes of their main hyperpolarizing peaks.

Earlier, experiments with fixed light spots were used to specify values for all adjustable model parameters (Table I). Using parameters from columns 4 and 3, and the measured velocity of the grating, model-predicted kernels (labeled "*b*" and "*c*", respectively, in Fig. 6) were calculated as explained below.

First, $\Psi(r,f)$ was computed from Eqs. A16 and B8 using the feedback kernel, $\hat{A}(f)\hat{k}(f)$, from Fig. 5 (wavy trace) in definitions from Eqs. A9 and A10 for γ and δ. Given $\Psi(r,f)$, the transform of the moving grating kernel, $\hat{V}(r,f)/\hat{i}(f)$, follows from Eq. 9 once $\hat{g}(f)\hat{A}(f)$ is known. The latter quantity is the expected light-to-horizontal cell transfer function in the absence of feedback, given either spot or field illumination. From Eq. 9:

$$\hat{g}(f)\hat{A}(f) = \frac{\hat{V}(r,f)/\hat{i}(f)}{m(\bar{I})\bar{I}\Psi(r,f)}, \tag{23}$$

where the numerator may be taken as the transform of the experimentally measured light-to-horizontal cell kernel and $\Psi(r,f)$ is given by the model solution in Eq. A23. The feedback-free horizontal cell kernel determined in this manner from Eq. 23 was similar to the actual spot kernel but slightly slower due to the small amount of feedback assumed to be activated by a 200 μm spot.

Returning to Fig. 6, notice that the model kernels, which were derived entirely from experimentation with spot and field stimuli, are good predictors of the moving grating kernel. We expect that the predictions would be even more accurate if both spot and grating experiments could be performed on the same cell during a single experiment. Possible errors of as much as 10% in the measurement of the grating velocity could also account for slight discrepancies.

As the bar velocity is increased, model-predicted moving grating kernels become faster as indicated in Fig. 7. The trace labeled *c* is identical to trace *b* in Fig. 6. Trace 2*c* is at twice the velocity, and so on. For slow grating speeds, the kernel amplitudes actually double each time the speed is doubled, but the kernels in Fig. 7 are scaled to circumvent this effect. As the bar velocity approaches infinity, predicted kernels become identical to the kernel for field illumination shown in Fig. 3. In the model equations, this corresponds to the fact that Eqs. B6 and 17 become equal when bar velocity, *c*, and spot radius, *R*, are both infinite. Since a bar moving across the retina at a very high velocity is equivalent to a brief flash of uniform field

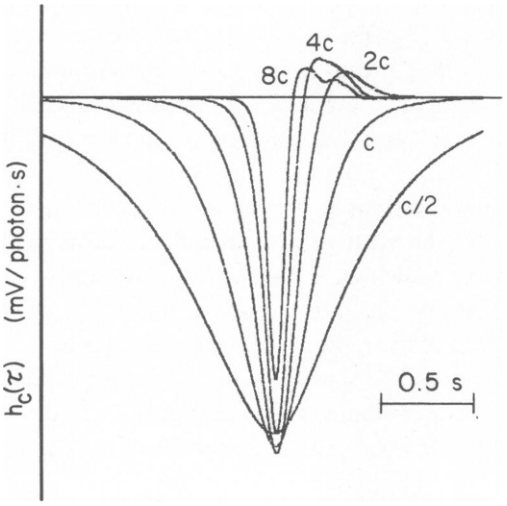

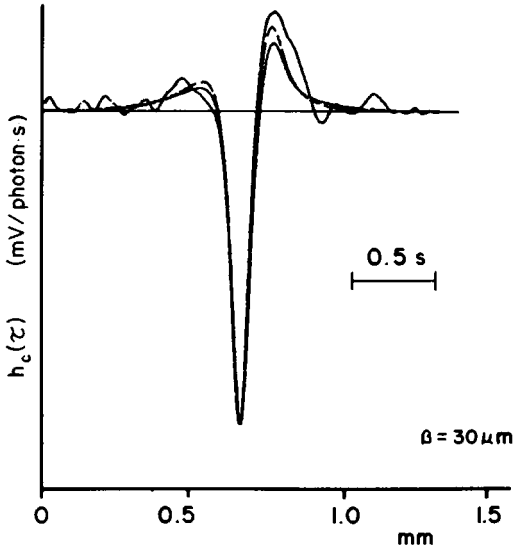

FIGURE 7

FIGURE 8

FIGURE 7 Effects of grating velocity. Model-predicted horizontal cell kernels for grating speeds $c/2$, $2c$, $4c$, and $8c$, where c is the velocity of the grating in the experiment of Fig. 6 *a* (0.57 mm/s). As velocity increases further, moving grating kernels approach the field kernel in Fig. 3 A.

FIGURE 8 Predicted receptor and experimental bipolar cell moving grating kernels. The smooth solid trace is the predicted receptor kernel based on Table I, column 4 parameters while the dashed trace assumes parameter values in column 3. The wavy kernel was measured from a bipolar cell and is corrected for the input autocorrelation.

illumination, the model kernels of Fig. 7 have the correct limiting behavior and resemble experimental observations.

Fig. 8 shows predicted receptor moving, grating kernels corresponding to the horizontal cell kernels in Fig. 6. The smooth, solid trace comes from parameters in Table I, column 4, whereas the dashed trace is predicted from column 3 parameters. Both assume a receptor coupling constant, β, of 30 μm. The model predicts a slight depolarizing surround, which has never been reported in catfish receptors. Rather, bipolar cells are believed to be the first to show a concentric receptive field organization.

The wavy trace in Fig. 8 is a typical moving, grating kernel for an off-center, bipolar cell and looks very much like the model receptor kernels, although the close quantitative agreement may be coincidental. This comparison is included for the sake of completeness, and demonstrates that a weakness of the subtractive feedback model is its prediction of bipolar-like receptive field properties for receptors.

DISCUSSION

We began with a set of hypotheses about receptor and horizontal cells and their mutual interaction, and formulated these hypotheses as a mathematical model. Now that the behavior of this model has been derived analytically and tested quantitatively, it is time to reexamine each hypothesis in light of experimental evidence.

Linearity

Previous studies have demonstrated nearly linear horizontal cell behavior for small modulations in light intensity about a mean (Marmarelis and Naka, 1973*a*).

The Michaelis relation between steady-state light intensity and mean potential (Marmarelis and Naka, 1972) is responsible for the appearance of some nonlinear effects as modulation depth increases. In a model of turtle photoreceptors (Baylor et al., 1974) the Michaelis relation is assumed to be a zero-memory type nonlinearity that follows initial linear stages of phototransduction.

It is a special property of Gaussian white-noise inputs that zero-memory nonlinearities interspersed between linear filters do not affect the overall input-output correlation (Korenberg, 1973; Marmarelis and Marmarelis, 1978). Therefore, by using white-noise inputs we are able to measure the small-signal, linear dynamics of horizontal cells even though the modulation amplitude required for a satisfactory output signal:noise ratio invokes some nonlinear behavior due to the Michaelis relation.

Independent Receptor Transduction

In the absence of feedback and coupling, the transfer function, $\hat{g}(f)$, of a single receptor is presumed to be independent of the activity of other receptors. In turtle retina the spectrum of photon noise recorded extracellularly from single cone outer segments does not depend on the area of the light stimulus (Lamb and Simon, 1977). It therefore seems justifiable to place coupling and feedback after phototransduction in Fig. 1.

Coupling between Horizontal Cells and between Receptors

Physiological evidence for coupling has already been mentioned. Anatomically, tight junctions have been found between horizontal cells (Yamada and Ishikawa, 1965; Witkovsky and Dowling, 1969) and close membrane appositions have been observed between catfish receptors (Witkovsky et. al., 1974).

Feedforward Connections

Horizontal cells are driven by receptors, and the near linearity of horizontal cell kernels argues that any filtering along this forward pathway must be nearly linear, as we have assumed. In retinas where both receptors and horizontal cells have been tested with the same stimulus, the time-course of horizontal cell response was similar to, but slightly slower than, the receptor response (Baylor et al., 1971; Burkhardt, 1977).

Horizontal Cell Feedback

Direct evidence for feedback from horizontal cells to receptors comes from experiments in turtle retina where current injected into a horizontal cell caused a response of opposite polarity in a nearby receptor (Baylor et. al., 1971). In the model we have tested, fluctuations in horizontal cell potential are passed through linear filters, and the result is subtracted from fluctuations in the response of nearby receptors. An increase in either the area or the modulation depth of a light stimulus causes a more extensive spread of horizontal cell potential fluctuations and, due to the uniform spatial distribution of the proposed feedback connections, more feedback paths are excited. Each feedback filter also sees a larger input due to the summation of S-potentials. Since feedback causes horizontal cell responses to become

faster, spatially distributed feedback paths cause responses to speed up with increasing stimulus area.

So distributed feedback connections are a natural way to explain the dependence of horizontal cell time-course on stimulus area. The assumption that horizontal cell potential is filtered linearly and subtracted from receptor potential keeps model responses linear for fluctuations about a mean. Such linear feedback may also be regarded as the first-order approximation to feedback dynamics in the case of a more complex nonlinear interaction.

Perhaps the strongest point in favor of our linear feedback model is the fact that the rather complicated field-to-spot transfer function of Fig. 4 is accounted for by feedback paths with PSP-shaped impulse responses (Fig. 5). A PSP is the impulse response or first kernel of a linear synapse made by a spike generating cell. Therefore, if horizontal cells make chemical synapses with receptors, the feedback kernel should look like a PSP, provided the mechanisms of transmission are not unlike those at more conventional synapses. The findings of a PSP-like waveform for the presumed feedback effects in catfish retina is therefore consistent with the idea of chemical synapses, although the time constants for the feedback kernel are considerably slower than those of most vertebrate PSP's.

Model parameter values estimated by fitting model expressions to experimental dat (Fig. 4) also compare reasonably well with other estimates of similar parameters. For example, the time-course of presumed feedback effects has been inferred from experiments in turtle retina by Baylor et al. (1971) and O'Bryan (1973). They measured the massed depolarizing effect of horizontal cells on receptors by applying steady light over a small (70 μm), central spot and then flashing illumination of the whole field. After the flash, the transient depolarization that arose from the steady receptor hyperpolarization was attributed to feedback. To judge from Fig. 11*b* of Baylor et al., the waveform of the depolarizing effect resembled a low-pass filtered version of our proposed feedback waveform (Fig. 5) and decayed with a time-constant on the order of 60 ms. It must be remembered that our feedback kernel represents the impulse response of feedback effects alone, whereas the receptor depolarization measured with a flash of annular illumination also includes the initial temporal filtering due to receptor transduction.

Our estimate of the space-constant, $\lambda(0)$, for the spread of steady-state, S-potentials depends both on membrane resistivity and on the strength of assumed feedback. Both may depend on the mean light level. Horizontal cell kernels are known to become faster at higher light levels (Marmarelis and Naka, 1973 *b*), so feedback gain may increase. From Eq. 13, an increase in feedback gain causes a decrease in the effective space-constant, $\lambda(f)$, but such a decrease could be offset by an increase in membrane resistivity. Marmarelis and Naka (1972) reported an increase in space-constant with brighter lights and suggested increased membrane resistivity as the reason. In spite of differences in experimental design, values of $\lambda(0)$ calculated from parameters in Table I were within the range of space-constants reported by Marmarelis and Naka (1972).

We have seen that the linear subtractive feedback model is quite successful at predicting the horizontal cell response to a moving grating but has a problem with receptors. A triphasic receptor kernel (Fig. 8) is predicted even if it is assumed that feedback is inactive in regions of darkness. Receptor coupling could obscure a depolarizing surround, but only if the receptor space-constant is assumed to be excessively large (>100 μm).

Alternatives to Subtractive Feedback

Without subtractive feedback, the area dependence of horizontal response waveforms must somehow be ascribed to dynamic properties of receptor or horizontal cell membranes, to coupling between cells, or to synaptic transmission from receptors to horizontal cells.

Membrane capacitance introduces dynamics into horizontal cell membranes and affects the spread of S-potential. However, we have already seen that horizontal cell capacitance acts oppositely to feedback in Eqs. 13 and 19, and causes kernels to become slower rather than faster with increasing stimulus area.

The addition of a capacitive component to the coupling between horizontal cells would cause the internal S-space resistivity, ρ_i, to be larger at higher frequencies. In view of Eqs. 4, 13, and 19, the space-constant will decrease, rather than increase, at higher frequencies, and kernels will again become slower instead of faster as stimulus area increases.

Changes in the dynamics of synaptic transmission from receptors to horizontal cells must be mediated by changes in either presynaptic or postsynaptic membrane potentials. Postsynaptic modifications would leave receptor waveforms unchanged as stimulus area increases. On the other hand, receptor coupling is not extensive enough for stimulus area to have much effect presynaptically. Having dismissed those alternatives that come to mind, we seem compelled to accept some form of feedback hypothesis.

In linear or first-order feedback, larger area stimuli cause faster horizontal cell kernels by increasing the amplitude and extent of potential fluctuations about the mean level of hyperpolarization. However, larger area stimuli also increase the hyperpolarization of horizontal cells, so an alternative hypothesis is that changes in kernel waveforms are somehow mediated by the mean level of horizontal cell potential itself rather than by fluctuations about the mean. This type of feedback, which we shall call "zero-order," has several advantages when compared with the linear subtractive feedback model.

(*a*) Since horizontal cell hyperpolarization increases as a light stimulus becomes either larger or brighter, zero-order feedback can account for the observation that kernels become faster in both cases. Linear feedback only produces faster kernels for brighter stimuli if forward or feedback gain increases.

(*b*) Zero-order feedback accounts for the finding that horizontal cell spot kernels become faster in the presence of a steady annulus of light (Marmarelis and Naka, 1973 *b*) since the annulus hyperpolarizes horizontal cells in the central spot region.

(*c*) Zero-order feedback does not create a depolarizing surround in receptors. This is consistent with the idea that the bipolar cell surround (Fig. 8) is formed by direct horizontal to bipolar pathways (Shantz and Naka, 1976).

It is therefore likely that the level of horizontal cell potential is a prime determinant of response dynamics, but the mechanism for such control needs to be clarified. If feedback is mediated by chemical synapses, as suggested earlier, then both mean horizontal cell potential and potential fluctuations will affect the amount of transmitter released. Consequent changes in receptor membrane conductance will mediate zero order, linear and higher-order feedback effects on receptor potential. The mechanism by which mean receptor conductance might determine response dynamics still remains a question. (We have merely replaced mean horizontal cell potential with mean receptor conductance as the zero-order controlling agent).

Whatever mechanism is proposed should account for the horizontal cell field-to-spot transfer function (Fig. 4) so conveniently fit by linear subtractive feedback.

Further progress at understanding the dynamic behavior of neural circuitry in the distal retina requires detailed analysis of both the time and voltage dependence of transduction, synaptic transmission, membrane conductances, and electrical coupling. Since realistic models that result from such an analysis must predict the spatiotemporal properties of horizontal and receptor cells, it is hoped that the techniques and formulas presented here will be of some use in their future development.

This research was supported by Department of Health, Education, and Welfare grant EY10897 and Department of Health, Education, and Welfare postdoctoral research fellowship NS05665 to Dr. Krausz.

Received for publication 31 January 1979 and in revised form 23 September 1979.

APPENDIX A: THE CASE OF COUPLED RECEPTORS

In this section we generalize the basic model Eqs. 10 and 11 and their solutions to incorporate receptor intercoupling and to allow for variation of parameter values between regions of light and darkness.

Lamb and Simon (1976) have considered various elecrical models of receptor coupling and have come to the conclusion that a laminar spread of potential analogous to the usual model of horizontal cell potential fits their receptor data as well as any other reasonable model. We therefore assume that the receptor layer behaves similarly to the S-space but with a different spread parameter, β. With this modification Eqs. 10 and 11 now become a pair of coupled Bessel equations:

$$\beta^2\nabla^2\Phi(r,f) - (1 + i2\pi c_r f)\phi(r,f) = -p(r) + \hat{k}(f)\hat{A}(f)\Psi(r,f) \tag{A1}$$

$$\alpha^2\nabla^2\Psi(r,f) - (1 + i2\pi c_s f)\Psi(r,f) = -\Phi(r,f), \tag{A2}$$

where c_r and c_s denote the product of membrane resistances and capacitances for receptor and horizontal cell layers, respectively. The earlier definitions of Φ, Ψ, and α still apply, but receptor coupling becomes a part of their interpretation.

In a more abbreviated operator notation, Eqs. A1 and A2 are equivalent to:

$$(\nabla^2 - q_r)\Phi = \frac{1}{\beta^2}[-p(r) + \hat{k}(f)\Psi(r,f)\hat{A}(f)] \tag{A3}$$

$$(\nabla^2 - q_s)\Psi = -\frac{\Phi}{\alpha^2}, \tag{A4}$$

where we define

$$q_r \doteq (1 + i2\pi c_r f)/\beta^2 \tag{A5}$$

$$q_s \doteq (1 + i2\pi c_s f)/\alpha^2. \tag{A6}$$

Substitution of Eq. A4 into Eq. A3 eliminates Φ from the two equations and following rearrangement leaves:

$$\left[(\nabla^2 - q_r)(\nabla^2 - q_s) + \frac{\hat{A}(f)\hat{k}(f)}{\alpha^2\beta^2}\right]\Psi(r,f) = \frac{p(r)}{\alpha^2\beta^2}. \tag{A7}$$

With an appropriate choice of two auxiliary spread parameters γ and δ, Eq. A7 can be put into the form:

$$\left(\nabla^2 - \frac{1}{\gamma^2}\right)\left(\nabla^2 - \frac{1}{\delta^2}\right) = \frac{p(r)}{\alpha^2\beta^2}. \tag{A8}$$

Equating coeffcients of like powers of ∇^2 between Eqs. A7 and Eq. A8 gives a pair of equations that determine γ and δ. These are:

$$\frac{1}{\gamma^2} + \frac{1}{\delta^2} = q_r + q_s$$

$$\frac{1}{\gamma^2\delta^2} = q_r q_s + \frac{\hat{A}(f)\hat{k}(f)}{\alpha^2\beta^2},$$

and their solution is

$$\gamma^2 = 2\left[q_r + q_s \pm \sqrt{(q_r - q_s)^2 - \frac{4\hat{A}(f)\hat{k}(f)}{\alpha^2\beta^2}}\right]^{-1} \tag{A9}$$

$$\delta^2 = 2\left[q_r + q_s \mp \sqrt{(q_r - q_s)^2 - \frac{4\hat{A}(f)\hat{k}(f)}{\alpha^2\beta^2}}\right]^{-1} \tag{A10}$$

Now to solve Eq. A8 for Ψ let $\chi(r, \gamma)$ satisfy

$$\left(\nabla^2 - \frac{1}{\gamma^2}\right)\chi(r, \gamma) = -p(r) \tag{A11}$$

From Eq. 15 we have:

$$\chi(r, \gamma) = \int_0^\infty p(s)G(r, s)s\,ds, \tag{A12}$$

with $G(r, s)$ given by Eq. 14. Let us also define $\chi(r, \gamma)$ as the solution to:

$$\left(\nabla^2 - \frac{1}{\delta^2}\right)\chi(r, \delta) = -p(r). \tag{A13}$$

Since the order of products on the left side of Eq. A8 is immaterial, direct comparisons of Eqs. A12 and A13 with Eq. A8 reveal that

$$\left(\nabla^2 - \frac{1}{\gamma^2}\right)\Psi = -\chi(r, \delta)/\alpha^2\beta^2, \tag{A14}$$

and

$$\left(\nabla^2 - \frac{1}{\delta^2}\right)\Psi = -\chi(r, \gamma)/\alpha^2\beta^2. \tag{A15}$$

Subtracting the second equation above from the first yields the solution

$$\Psi(r, f) = \frac{1}{\alpha^2\beta^2}\left(\frac{\gamma^2\delta^2}{\gamma^2 - \delta^2}\right)[\chi(r, \gamma) - \chi(r, \delta)]. \tag{A16}$$

Notice that Eq. A16 is a general solution for $\Psi(r, f)$ and does not depend on the particular pattern, $p(r)$, of the light stimulus. In the case of a uniformly illuminated circular spot of radius R,

$$\chi(r, \gamma) = F(r, R, \gamma),$$

and

$$\chi(r, \delta) = F(r, R, \delta),$$

where $F(r, R, \lambda)$ is the function defined by Eq. 17.

To solve for the receptor transfer function $\Phi(r, f)$, we return to Eq. A4 and substitute for $\nabla^2\Psi$ using Eq. A15. This gives:

$$\Phi = \alpha^2\left(q_s - \frac{1}{\delta^2}\right)\Psi + \chi(r, \gamma)/\beta^2.$$

Finally, putting in the solution for Ψ from Eq. A16 and simplifying yields the conclusion:

$$\Phi(r, f) = \frac{1}{\beta^2}\left(\frac{\gamma^2\delta^2}{\gamma^2 - \delta^2}\right)\left[\left(q_s - \frac{1}{\gamma^2}\right)\chi(r, \gamma) - \left(q_s - \frac{1}{\delta^2}\right)\chi(r, \delta)\right]. \tag{A17}$$

A further generalization of Eqs. A16 and A17 arises when parameter values may be different inside and outside the stimulus pattern. It is prohibitively difficult if not impossible to solve even the basic model, Eq. 12, when α and $\lambda(f)$ are general functions of r. However, the problem can be solved in a piecewise fashion when the analysis is restricted to uniformly illuminated circular spot stimuli. Following the approach of Naka and Rushton (1967) we assume that α and $\lambda(f)$ are constant inside or outside of the light spot, but that their respective values differ between the two regions. Under these assumptions the basic Eq. 12 becomes:

$$\nabla^2\Psi - \frac{1}{\lambda_1^2}\Psi = -\frac{1}{\alpha_1^2} \qquad r < R$$

$$\nabla^2\Psi - \frac{1}{\lambda_2^2}\Psi = 0 \qquad r > R, \tag{A18}$$

where parameters with subscript 1 refer to values in light regions and subscript 2 values apply in darkness.

To solve Eq. A18 we use the fact that

$$\Psi(r, f) = c_1 I_0(r/\lambda_1) + \frac{\lambda_1^2}{\alpha_1^2} \tag{A19}$$

is a general solution to Eq. A18 for $r < R$, and remains finite when $r = 0$. In the region outside the spot ($r > R$),

$$\Psi(r, f) = c_2 K_0(r/\lambda_2) \tag{A20}$$

is a general solution that approaches zero as r approaches infinity.

Following Naka and Rushton, constants c_1 and c_2 are chosen so that $\Psi(r, f)$ will be continuous and have a continuous first derivative at the boundary $r = R$. The result is:

$$\Psi(r, f) = \frac{1}{\alpha_1^2} F(r, R, \lambda_1, \lambda_2), \tag{A21}$$

where

$$F(r, R, \lambda_1, \lambda_2) = \begin{cases} \lambda_1^2\left(1 - \dfrac{\xi(R)}{\lambda_2}\right) I_0(r/\lambda_1)K_1(R/\lambda_2) & r < R \\ \lambda_1 \xi(R) I_1(R/\lambda_1) K_0(r/\lambda_2) & r > R \end{cases}$$

and

$$\xi(R) = \left[\frac{1}{\lambda_1} I_1(R/\lambda_1)K_0(R/\lambda_2) + \frac{1}{\lambda_2} I_0(R/\lambda_1)K_1(R/\lambda_2)\right]^{-1}.$$

When $\lambda_1 = \lambda_2$, $\xi(R) = R$ and Eq. A21 reduces to the formula of Eq. 17 for $F(r, R, \lambda)$ as it must.

The comparatively simple result Eq. A21 is of use in the more complex case of coupled receptors. When γ and δ take different values inside and outside of a light spot, Eq. A8 becomes:

$$\left(\nabla^2 - \frac{1}{\gamma_1^2}\right)\left(\nabla^2 - \frac{1}{\delta_1^2}\right)\Psi = \frac{1}{\alpha_1^2\beta_1^2} \qquad r < R$$

$$\left(\nabla^2 - \frac{1}{\gamma_2^2}\right)\left(\nabla^2 - \frac{1}{\delta_2^2}\right)\Psi = 0 \qquad r > R. \tag{A22}$$

Using exactly the same steps, Eqs. All–A15, that were used to derive Eq. A16, but treating the light and dark regions separately, it can be shown that Eq. A16 generalizes to:

$$\Psi(r, f) = \frac{1}{\alpha_1^2\beta_1^2}\left(\frac{\gamma_i^2\delta_i^2}{\gamma_i^2 - \delta_i^2}\right)\left[\begin{matrix} F(r, R, \gamma_1, \gamma_2) - \\ F(r, R, \delta_1, \delta_2) \end{matrix}\right],$$

where

$$i = \begin{cases} 1 & r < R \\ 2 & r > R. \end{cases} \tag{A23}$$

An analagous generalization applies to the receptor formula of Eq. A17.

APPENDIX B: MOVING RECTILINEAR STIMULI

The theoretical section of this paper formulates a linear spatiotemporal model of horizontal cell responses and derives their frequency response given an arbitrary radially symmetric stimulus pattern, $p(r)$, in terms of the impulse response or Green's function, $G(r, s)$. The horizontal cell frequency response function $\Psi(r, f)$ defined by Eq. 9 is determined by the convolution integral, Eq. 15.

In this appendix, the convolution formula (Eq. 15) for radial stimuli is generalized to the case of one dimensional rectilinear stimuli. At the center of a radial stimulus pattern Eq. 15 becomes:

$$\Psi(0, f) = \Psi(f) = \frac{1}{\alpha^2}\int_0^\infty p(s)G(0, s)\, s\,ds$$

$$= \int_0^\infty p(s)\frac{K_0(s/\lambda)}{\alpha^2}\, s\,ds$$

$$\Psi(f) = \int_0^{2\pi}\int_0^\infty p(s)\left[\frac{K_0(s/\lambda)}{2\pi\alpha^2}\right] s\,ds\,d\theta. \tag{B1}$$

The last equation above is an integral over all space, and serves to identify the quantity in brackets as the spatiotemporal impulse response.

In its current form Eq. B1 still applies only to fixed intensity modulated stimulus patterns, but this is overly restrictive. Making use of the definition of $\Psi(f)$ we may write:

$$\frac{V(f)}{m(\bar{I})\hat{g}(f)A(f)} = \frac{1}{2\pi\alpha^2}\int_0^{2\pi}\int_0^{\infty}\hat{I}(f,r,\theta)K_0(r/\lambda)\,r\mathrm{d}r\mathrm{d}\theta, \tag{B2}$$

where $\hat{I}(f,r,\theta)$ is now a light stimulus that depends in a general way on both temporal frequency and spatial location. Moving stimuli are a common example.

Let us now consider a one dimensional, rectilinear stimulus pattern moving at constant velocity, c. In an x-y-coordinate system we assume the pattern varies in the x direction but not along the y axis. Motion is also along the x axis. Therefore the stimulus intensity as a function of time and space is

$$I(t,r,\theta) = I(t,x,y) = \bar{I}\cdot i(t - x/c),$$

where $i(t)$ is the intensity modulation signal at the arbitrary origin.

The horizontal cell response to a moving stimulus is predicted by Eq. A2 after the stimulus is Fourier transformed and converted to polar coordinates. From the shift theorem of Fourier transforms (Bracewell, 1969),

$$\hat{I}(f,x) = \bar{I}_i(f)e^{-i2\pi fx/c}.$$

Substituting $x = r\cos\theta$ gives:

$$\hat{I}(f,r,\theta) = \bar{I}_i(f)e^{-i2\pi(f/c)r\cos\theta}. \tag{B3}$$

Substitution of Eq. B3 for $I(f,r,\theta)$ in Eq. B2 gives

$$\frac{\hat{V}(f)}{m(\bar{I})\bar{I}\hat{g}(f)\hat{A}(f)} = \frac{1}{\alpha^2}\hat{\imath}(f)\int_0^{\infty}\left[\frac{1}{2\pi}\int_0^{2\pi}e^{-i2\pi(f/c)r\cos\theta}\,\alpha\theta\right]K_0(r/\lambda)\,\mathrm{d}r. \tag{B4}$$

The quantity in brackets is one of the definitions of the Bessel function $J_0(2\pi fr/c)$. Therefore,

$$\frac{\hat{V}(f)/\hat{\imath}(f)}{m(\bar{I})\bar{I}\hat{g}(f)\hat{A}(f)} = \Psi_c(f) = \frac{1}{\alpha^2}\int_0^{\infty}J_0(2\pi fr/c)K_0(r/\lambda)\,r\mathrm{d}r. \tag{B5}$$

The ratio $\hat{V}(f)/\hat{\imath}(f)$ is simply the transfer function between the light stimulus signal $i(t)$ and the horizontal cell response at the origin of the coordinate system. With appropriate choice of origin, this transfer function is the transform of the horizontal cell kernel measured with a white-noise grating moving at velocity c (Fig. 6).

The integral on the right side of Eq. B5 is the Hankel transform of the function $K_0(r/\lambda)$. Hankel transforms are analogous to two dimensional Fourier transforms, but arise in problems with radial symmetry. A table of Hankel transforms (Bracewell, 1969) reduces Eq. B5 to:

$$\Psi_c(f) = \left(\frac{\lambda}{\alpha}\right)^2\frac{1}{1 + (2\pi f\lambda/c)^2}. \tag{B6}$$

The formula of Eq. B6 is the desired extension of the basic model solution (Eq. 17) to moving one dimensional stimuli. Note the analogy between $\lambda^2[1 + (2\pi f\lambda/c)^2]^{-1}$ in Eq. B6 and $F(r, R, \lambda)$ in Eq. 17.

The equation for the receptor cell layer transfer function follows from the fact that receptor potential $\hat{U}(f)$ is:

$$\hat{U}(r,f) = m(\bar{I})\hat{I}(f,r,\theta)\hat{g}(f) - \hat{k}(f)\hat{V}(r,f),$$

so

$$\Phi_c(f) = \frac{\hat{U}(f)/\hat{i}(f)}{m(\bar{I})\bar{I}\hat{g}(f)} = 1 - \left(\frac{\lambda}{\alpha}\right)^2 \frac{\hat{A}(f)\hat{k}(f)}{1 + (2\pi f\lambda/c)^2}. \tag{B7}$$

Both Eqs. B6 and B7 neglect any effects of receptor coupling. In Appendix A, formulas in Eqs. A16 and A17 are derived for $\Psi(f)$ and $\Phi(f)$. These formulas include the effects of receptor coupling and depend on the basic solutions for $\chi(r, \gamma)$ and $\chi(r, \delta)$ given by Eq. A2. In the case of spot illumination, $\chi(r, \gamma) = F(r, R, \gamma)$, as defined by Eq. 17 or A21. For moving one dimensional stimuli we have just seen that $\lambda^2[1 + (2\pi f\lambda/c)^2]^{-1}$ replaces $F(r, R, \lambda)$, so formulas in Eqs. A16 and A17 apply to moving stimuli when:

$$\chi(r, \gamma) = \gamma^2[1 + (2\pi f\gamma/c)^2]^{-1}$$

and

$$\chi(r, \delta) = \delta^2[1 + (2\pi f\delta/c)^2]^{-1}. \tag{B8}$$

We conclude this section with the observation that Eqs. A16 and A17 constitute a perfectly general solution to the linear dynamic problem of potential flow in two coupled cell layers connected by reciprocal pathways. The response of either cell layer to any stimulus $I(t, r, \theta)$ is determined by these formulas once $\chi(r, \lambda)$ is found from the convolution of $I(f, r, \theta)$ with $K_0(r/\lambda)$.

REFERENCES

ABRAMOWITZ, M., and I. A. STEGUN, editors. 1965. Handbook of Mathematical Functions with Formulas, Graphs and Mathematical Tables. Dover Publications, New York.

BAYLOR, D. A., M. G. F. FUORTES, and P. M. O'BRYAN. 1971. Receptive fields of cones in the retina of the turtle. *J. Physiol. (Lond.).* **214**:265–294.

BAYLOR, D. A., A. L. HODGKIN, and T. D. LAMB. 1974. The electrical response of turtle cones to flashes and steps of light. *J. Physiol. (Lond.).* **242**:685–727.

BRACEWELL, R. 1965. The Fourier Transform and Its Applications. McGraw-Hill Book Co., Inc., New York.

BROWN, K. M.,and J. E. DENNIS. 1972. Derivative free analogues of the Levenberg-Marquardt and Gauss algorithms for nonlinear least squares approximation. *Numer. Math.* **18**:289–297.

BURKHARDT, D. A. 1977. Responses and receptive-field organization of cones in Perch retinas. *J. Neurophysiol. (Bethesda).* **40**:53–62.

CARSLAW, H. S., and J. C. JAEGER. 1959. Conduction of Heat in Solids. Clarendon Press, Oxford, England. 2nd edition.

DETTMAN, J. W. 1969. Mathematical Methods in Physics and Enginering. McGraw-Hill Book Co., New York. 2nd edition.

FUKAROTANI, K., and K.-I. HARA. 1975. A dynamic model of the receptive field of C-cells in the carp retina. *Biol. Cybern.* **20**:1–8.

JACK, J. J. B., D. NOBLE, and R. W. TSIEN. 1975. Electrical current flow in excitable cells. Clarendon Press. Oxford, England.

KORENBERG, M. J. 1973. Cross-correlation analysis of neural cascades. *Proc. 10th Ann. Rocky Mountain Bioengr. Symp.* 47–51.

KREIDER, D. L., R. G. KULLER, D. R. OSTBERG, and F. W. PERKINS. 1966. An Introduction to Linear Analysis. Addison-Wesley Publishing Co., Inc., Reading, Mass.

LAMB, T. D. 1976. Spatial properties of horizontal cell responses in the turtle retina. *J. Physiol. (Lond.).* **263**:239–255.

LAMB, T. D., and E. J. SIMON, 1976. The relation between intercellular coupling and electrical noise in turtle photoreceptors. *J. Physiol. (Lond.).* **263**:257–286.

LAMB, T. D., and E. J. SIMON, 1977. Analysis of electrical noise in turtle cones. *J. Physiol. (Lond.).* **272**:435–468.

LEE, Y. W., and M. SCHETZEN. 1965. Measurement of the Wiener kernels of a nonlinear system by crosscorrelation. *Int. J. Control.* **2**:237–254.

MARMARELIS, R. Z., and K.-I. NAKA. 1972. Spatial distribution of potential in a flat cell: application to the catfish horizontal cell layers. *Biophys. J.* **12**:1515–1532.

MARMARELIS, P. Z., and K.-I. NAKA. 1973a. Nonlinear analysis and synthesis of receptive field responses in the catfish retina II. One-input white-noise analysis. *J. Neurophysiol.* **36**:619–633.

MARMARELIS, P. Z., and K.-I. NAKA. 1973*b*. Nonlinear analysis and synthesis of receptive field responses in the catfish retina III. Two-input white-noise analysis. *J. Neurophysiol.* **36**:634–648.

MARMARELIS, P. Z., and K.-I. NAKA. 1974. Experimental analysis of a neural system: two modelling approaches. *Kybernetic.* **15**:11–26.

MARMARELIS, P. Z., and V. Z. MARMARELIS. 1978. The Analysis of Physiological Systems. Plenum Publishing Co., New York.

NAKA, K.-I., and P. W. NYE. 1970. Receptive-field organization of the catfish retina: are at least two lateral mechanisms involved? *J. Neurophysiol.* **33**:625–642.

NAKA, K.-I., and W. A. H. RUSHTON. 1967. The generation and spread of S-potentials in fish (Cyprinidae). *J. Physiol. (Lond.).* **192**:437–461.

NELSON, R. 1977. Cat cones have rod input: a comparison of the response properties of cones and horizontal cell bodies in the retina of cat. *J. Comp. Neurol.* **172**:109–135.

O'BRYAN, P. M. 1973. Properties of the depolarizing synaptic potential evoked by peripheral illumination in cones of the turtle retina. *J. Physiol. (Lond.).* **235**:207–223.

SHANTZ, M. J., and K.-I. NAKA. 1976. The bipolar cell. *Vision Res.* **16**:1517–1518.

TOYODA, J. 1974. Frequency characteristics of retinal neurons in the carp. *J. Gen. Physiol.* **63**:214–234.

WITKOVSKY, P., and J. E. DOWLING. 1969. Synaptic relationships in the plexiform layers of carp retina. *Histochemie.* **100**:60–82.

WITKOVSKY, P., M. SHAKIB, and H. RIPPS. 1974. Interreceptoral junctions in the teleost retina. *Invest. Ophthalmol.* **13**:996–1009.

YAMADA, E., and T. ISHIKAWA. 1965. Fine structure of horizontal cells in some vertebrate retinae. *Cold Spring Harbor Symp. Quant. Biol.* **30**:383–392.

YASUI, S., W. DAVIS, and K. I. NAKA. 1979. Spatio-temporal receptive field measurement of retinal neurons by random stimulation and cross-correlation. *IEEE Transactions on Biomedical Engineering.* **BME-26**:263–272.